Heliyon

A novel type of semi-active jet turbulence grid

N. Szaszák [a,*]**, C. Roloff** [b]**, R. Bordás** [b,c]**, P. Bencs** [a]**, S. Szabó** [a]**, D. Thévenin** [b]

[a] *Department of Fluid and Heat Engineering, Institute of Energy Engineering and Chemical Machinery, University of Miskolc, Miskolc-Egyetemváros, H-3515, Hungary*

[b] *Lab. of Fluid Dynamics & Technical Flows, University of Magdeburg "Otto von Guericke", Universitätsplatz 2, Magdeburg, D-39106, Germany*

[c] *Now at IAV GmbH, Germany*

* Corresponding author.
E-mail address: aramszn@uni-miskolc.hu (N. Szaszák).

Abstract

This article describes a novel approach to generate increased turbulence levels in an incoming flow. It relies on a cost-effective and robust semi-active jet grid, equipped with flexible tubes as moving elements attached onto tube connections placed at the intersections of a fixed, regular grid. For the present study, these flexible tubes are oriented in counter-flow direction in a wind tunnel. Tube motion is governed by multiple interactions between the main flow and the jets exiting the tubes, resulting in chaotic velocity fluctuations and high turbulence intensities in the test section. After describing the structure of the turbulence generator, the turbulent properties of the airflow downstream of the grid in both passive and active modes are measured by hot-wire anemometry and compared with one another. When activating the turbulence generator, turbulence intensity, turbulent kinetic energy, and the Taylor Reynolds number are noticeably increased in comparison with the passive mode (corresponding to simple grid turbulence). Furthermore, the inertial subrange of the turbulent energy spectrum becomes wider and closely follows Kolmogorov's -5/3 law. These results show that the semi-active grid, in contrast to passive systems, is capable of producing high turbulence levels, even at low incoming flow velocity. Compared to alternatives based on actuators driven by servo-motors,

the production and operation costs of the semi-active grid are very moderate and its robustness is much higher.

Keyword: Mechanical engineering

1. Introduction

Passive grids for turbulence generation in wind tunnels have been widely used both in scientific projects as well as in practical engineering applications. Primarily, these grids are utilized to produce turbulence in the test section of wind tunnels just after the grid. Alternatively, when the inlet flow is already of high turbulence intensity but the velocity distribution is non-homogeneous over the cross section, grids have also been employed to improve flow quality and homogeneity. Passive grids simply represent an obstacle to the flow and do not move. However, they are sometimes called active grids in a general dynamic sense (Gad-el-Hak and Corrsin, 1974); e.g., the boundary layer separation lines move in an unsteady manner. In this article, however, they will systematically be called passive grids in order to avoid confusion.

A vast majority of all experiments on isotropic turbulence in wind tunnels (beginning perhaps with Simmons and Salter, 1934) have been carried out using such passive grids. Comte-Bellot and Corrsin (1966) investigated the role of a downstream contraction concerning isotropy of turbulence induced by passive grids. A systematic description of turbulence properties generated by passive grids is presented in Comte-Bellot (1971). Studies based on grid-generated turbulence have been essential in developing turbulence theories, models, and even measurement techniques (Sakai et al., 2001), as well as in delivering suitable boundary conditions and validation data. The Taylor Reynolds number (Re_λ) depends on the wire dimensions and should be sufficiently high to generate turbulence with realistic features (Kurian and Fransson, 2009). However, the turbulence level attainable with passive grids is limited by the dimensions of the test section and by the incoming flow velocity, since these grids merely convert part of the incoming flow energy into turbulent kinetic energy.

For this reason, more recent experiments have often applied *active grids*. This name is used here for two distinct categories: 1) grids with moving elements in the flow, such as vibrating grids (Ling and Wan, 1972; Sato and Saito, 1974), or 2) elements that are capable of adding additional momentum to the fluid (Ozono et al., 2007). As another alternative, grids that eject secondary fluid jets into the mean flow, called *jet grids*, have also shown promising potential (Gad-el-Hak and Corrsin, 1974; Aufderheide et al., 2014). Jet grids generate turbulence at higher intensities, but must still preserve a reasonable level of homogeneity, constraining the size of the test section and the mean flow velocities. They induce higher Reynolds numbers

and can thus be employed to extend the operating range of an existing setup (Kang et al., 2003).

The most common active grids are probably those with rotating vanes, first introduced by Makita and Miyamoto (1983). A detailed study describing the characteristics of the induced turbulence can be found in Makita (1991). The obtained properties were later compared with the results of a large-eddy simulation by Kang et al. (2003). Hearst and Lavoie (2015) provide an expansive parametric study of various grid parameters. Weitemeyer et al. (2013) compared their own experimental results for an active grid with results of fractal-type passive grids. Larssen and Devenport (2011) have most likely built the largest grid according to this concept and gave a comprehensive overview regarding grid turbulence, together with extensive experiments for many operating conditions. Probably the most recent paper reviewing the research related to "Makita-type" active grids is by Mydlarski (2017).

Concerning jet grids, Mathieu and Alcaraz (1965) in all likelihood first applied a jet grid, as reported by Gad-el-Hak and Corrsin (1974) and by Vonlanthen and Monkewitz (2011). The results of their experiment and of later ones (Guillon, 1968; Charnay, 1969) showed that jet grids can generate relatively high turbulence levels. To drive his wind tunnel, Teunissen (1969) also used a jet grid. This construction enabled the generation of turbulence with an arbitrary mean velocity. Luxenberg and Wiskind (1969) studied turbulence isotropy behind a jet grid. Many investigations have shown that, although the turbulence intensity is satisfactory, the obtained homogeneity is very often poor. Therefore, various attempts have been documented to increase homogeneity downstream of jet grids (Liu et al., 1971; Gad-el-Hak and Corrsin, 1974; Tassa and Kamotani, 1975; Hwang and Eaton, 2004; Fransson et al., 2005; Goepfert et al., 2010; Vonlanthen and Monkewitz, 2011). Another application of the jet grid was described by Variano et al. (2004). Inspired by the study of Mydlarski and Warhaft (1996) and Hwang and Eaton (2004), they used randomly-driven jets to generate turbulence in a tank.

The original challenge for the present work was the generation of high turbulence levels in a mean flow with low velocity, as typically encountered, for instance, in clouds, where low average speeds coincide with a comparatively large turbulence intensity (Bordás et al., 2013). A first attempt combined a passive grid with fast variations of the fan rotational speed used to generate the mean flow in the wind tunnel (Bordás et al., 2011). However, the obtained velocity fluctuations occurred on an unacceptably long time scale. Therefore, an active grid should have been used instead, but existing concepts were too expensive or not suitable for the project. Thus, an alternative had to be developed. After many unsuccessful attempts, the best concept was finally found as a cost-efficient modification of the jet grid toward a semi-active system, allowing the flow itself to drive the movements of flexible elements. Based

on these observations, the present article introduces a novel type of semi-active grid, based on a jet grid in counter-flow direction, with the jets exiting from flexible tubes attached to the intersections of a fixed grid. The multiple interactions between the incoming mean flow and the many jets result in the tubes exhibiting chaotic movements. As a result, high turbulence levels and very good homogeneity can be obtained with an inexpensive and robust installation.

The following presents the structure of the turbulence generator, the experimental setup, the results of the wind tunnel investigation, and comparisons between passive and active modes.

2. Instrumentation

A mean airflow was first generated using the conventional wind tunnel at the University of Miskolc (Hungary), with test section dimensions of $500 \times 500 \times 1500$ mm. The wind tunnel was operated in open-loop mode to eliminate any temperature change that could arise when closing the loop. During the measurements, four different mean flow (also called reference) velocities (U_{ref}) were set in the test section to the values of 3 m/s, 4 m/s, 5 m/s, and 6 m/s. In the passive mode, a fixed standard grid with a mesh spacing $M = 25$ mm was employed, leading to grid Reynolds numbers $U_{ref}M/\nu$ of 4.8×10^3, 6.4×10^3, 8×10^3, and 9.6×10^3, respectively. Here, the flexible tubes were not alimented and were simply pushed flush with the surface of the fixed grid by the incoming flow. Fig. 1 shows the test section including the grid, the experimental setup, and the location of the measurement points and lines, as discussed later.
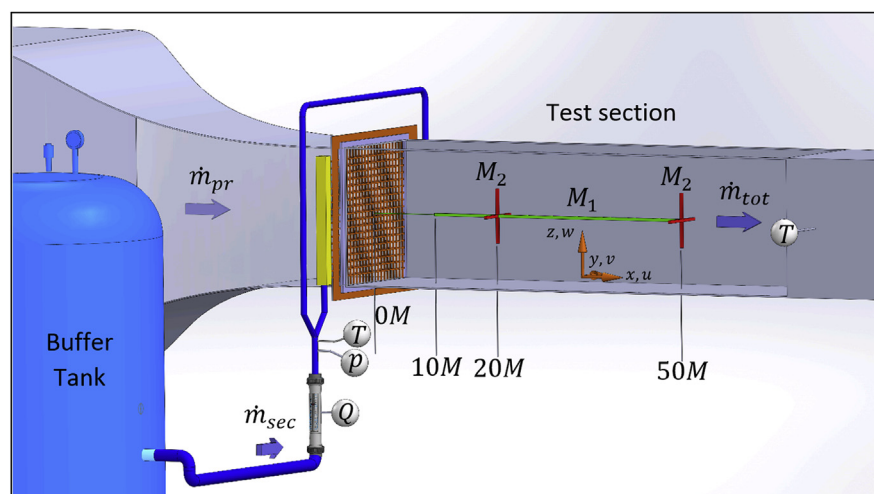

Fig. 1. Experimental setup with a zoom on the test section, including the reference system as well as measurement points and lines discussed later in the text.

In semi-active mode, the flexible tubes fixed onto the grid were supplied with pressurized air at a constant gauge pressure of 0.5 bar, measured just upstream of the Y manifold. In this mode, all flexible tubes flapped randomly due to the multiple interactions between the jets and the mean flow.

The grid was installed downstream of the contraction of the wind tunnel, just at the beginning of the test section. Therefore, no additional contraction was employed to further improve isotropy behind the grid in contrast to many other studies, e.g. Townsend (1954), Comte-Bellot and Corrsin (1966), or Antonia et al. (2010).

All measurements were carried out by means of the hot-wire measurement technique. A constant-temperature anemometer (CTA, from Dantec Dynamics, with 2 channels) was employed for all experiments. For a proper acquisition of turbulent properties, a two-dimensional nickel-coated fiber-film X-probe (type 55R51) was used, with 70 μm wire diameter (quartz fiber with 0.5 μm nickel coating), active sensor length of 1.25 mm and a wire separation of 1 mm. Both velocity and directional calibration of the X-probe were performed applying the computer controlled DANTEC Dynamics StreamLine Pro calibrator unit equipped with pitch-yaw manipulator. Based on the square-wave test built in the software, the assembled system is found to have a frequency response in excess of 20 kHz in the investigated velocity range. Overheat ratio was chosen to be 0.8. Accordingly to our later results the ratio of the wire separation to the Kolmogorov length scale varied between 5.3 (at $x/M = 10$) and 3.1 (at $x/M = 50$). Using this calibrated probe, both the streamwise (u) and the transverse, horizontal (v) instantaneous velocity components were measured simultaneously. The probe was fixed on a three-dimensional, computer-controlled positioning traverse system. To avoid any perturbation of the flow in the test section, the traverse system was placed outside the wind tunnel; only the probe with its support arm was introduced in the measurement section. The analog signals were then digitalized by a NI MIO 16 bit A/D converter and finally acquired with Dantec Streamware® 4.10 software. The resulting time-series of instantaneous velocity-component samples (in longitudinal as well as in transversal direction) were then processed using MATLAB scripts developed specifically for the purpose of this study (Szaszák et al., 2017). Based on recommendations from the literature, the measuring points were located downstream of the grid starting at a distance of $10M$. After verifying that isotropy can be assumed, the root-mean-square values of the transverse fluctuating velocity components can be considered approximately equal: $v_{rms} \approx w_{rms}$, where v and w are, respectively, the horizontal and vertical fluctuating velocity components, perpendicular to the main flow, as shown in Fig. 1. This assumption will later be applied for further post-processing.

Two different sets of measurement points (see again Fig. 1) were considered during this study:

- M1: Turbulence quantities downstream of the grid were measured along the centerline of the test section from $x = 10M-50M$ with steps of $5M$ (leading to 9 measurement points). The sampling frequency was set to $f_s = 20$ kHz (a low-pass filter of 10 kHz was applied) in order to attain a high resolution even for small-scale eddies in the flow. At each measurement point, the acquisition time was set to $t_s = 60$ s. This value was selected by increasing it progressively in steps of 10 s until changes below 1% were observed.

- M2: Furthermore, to investigate the homogeneity of the flow, the turbulence properties were measured at a fixed distance from the grid along one vertical (z) and one horizontal (y) line over a length of 200 mm, both crossing the centerline of the test section at distances of either $x = 20M$ or $50M$ (shown as two red crosses in Fig. 1). For these measurements, the reference velocity was set to U_{ref} = 4 m/s, and a spatial resolution of $1M$ was selected.

3. Design

After numerous preliminary investigations, it was finally possible to design a novel semi-active grid, which relies in its active state both on the impulse of multiple interacting secondary air jets and on the chaotic motion of elastic tubes to induce high velocity fluctuations. Consequently, a high level of turbulence can be achieved in the main flow, even at relatively low incoming velocities. Many different flexible tubes and operation parameters were examined (Szaszák et al., 2012) in order to obtain the highest increase in turbulence level, compared to the passive mode. The finally retained grid (Fig. 2) consisted of 20 pieces of horizontal and 20 pieces of vertical rectangular hollow brass rods with a wall thickness of 0.45 mm, soldered perpendicular to each other to form a biplane grid using a uniform rectangular pattern. The grid size was $M = 25$ mm with a rod thickness of 5 mm, resulting in a solidity ratio of $\sigma = 0.36$, which is nearly the same value as that used by Comte-Bellot and
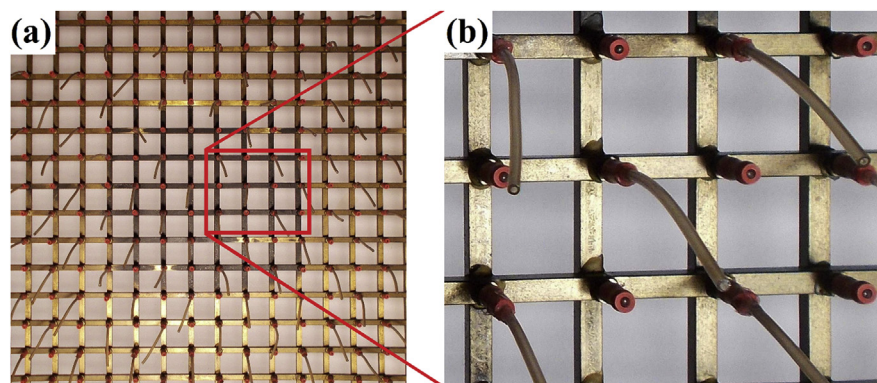

Fig. 2. (a) semi-active jet grid before starting the operation; (b) flexible tube elements and closed orifices shown for an enlarged view of part of the grid.

Corrsin (1966) for their square bar grids ($\sigma = 0.34$ in their experiments). In the case of conventional grids, the solidity has to be maintained well below a value of 0.5 to avoid the formation of an inhomogeneous flow field downstream of the grid (Villermaux et al., 1991).

In order to increase further turbulence intensity, pressurized air (later referred to as "secondary" air or flow) was injected into the grid through the horizontal hollow brass profiles. The air is then injected into the test section in counter-flow direction through soldered orifices with an inner diameter of 3 mm, onto which flexible tubes are attached. The number of active jets must be adjusted depending on the available volumetric flow rate of compressed air. For all experiments described in this work, a 3-phase open-piston compressor driven by an AC motor BOCK F16/2050NH (Q_{max} = 178.4 m^3/h and $p_{g,max}$ = 25 bar at n = 1450 r.p.m.) with a buffer tank of V_b = 0.315 m^3 was used to produce the pressurized air. After many tests, it was found that stable long-term operation was best obtained when every second junction point of the grid (shifted by one in each row, see Fig. 2b) was opened and connected to a flexible tube, while its four direct horizontal and vertical neighbors were closed. As a consequence, for all measurements discussed in what follows, each row of the fixed grid was finally associated to 10 air jets, and each column to 9 jets. In order to ensure the same volumetric flow rate for each jet, pressure losses within the grid were minimized by the following approach: two identical manifolds were mounted on the right-hand and on the left-hand sides of the grid (outside the wind tunnel, see Fig. 1), to which the above-mentioned 10 horizontal rods were directly connected. For one manifold, the pressurized air connection was fitted at the top; for the other, the connection to the piston compressor was connected at the bottom. With this technical solution, the total pressure drop was found to be nearly identical for all tubes. This is obviously necessary to ensure homogeneous turbulent conditions.

A gauge pressure of 0.5 bar (measured by a Testo 445 digital measuring unit with a Testo 0638.1645 pressure probe) was set at the inlet of the Y-manifold from which two tubes led to the two distribution manifolds on the right-hand and on the left-hand sides of the grid. The Y-manifold started behind the rotameter (type LZT G-25, Q_{max} = 160 m^3/h) used to measure the secondary volumetric flow rate. Additionally, the temperature of the secondary airflow behind the pressure gauge point was measured by a TECPEL DTM-800 digital thermometer with a K-type probe. Based on the measured quantities of the secondary flow, for all active-grid investigations described in this work, the secondary mass flow-rate $\dot{m}_{sec}$ was set to a value of 140 kg/h with a measured variation below 1.1 kg/h (less than 0.8% relative variation).

The relation between the mean velocity at $x/M = 50$ in the centerline of the wind tunnel (measured by CTA probe) and the volumetric flow rate through the whole test section was determined using a Pitot tube, based on the ISO 3966:2008 standard (velocity area method). Downstream of the test section, a temperature probe (Testo

445 mounted with a 0600-0493/411 sensor) was employed to measure the temperature of the flow at a distance $x/M = 77$; in addition, a DPI 145 sensor was utilized to measure the atmospheric pressure. The collected data enabled the calculation of the total mass flow rate through the test section ($\dot{m}_{tot}$). Knowing both the mass flow rate of the secondary airflow and the total mass flow rate in the test section, the ratio between these values could be determined. In semi-active mode, the values of the mass flow rate ratio $\dot{m}_{sec}/\dot{m}_{tot}$ were 4.1%, 3.2%, 2.6%, 2.2%, corresponding to mean velocity in the test section (U_{ref}) of 3 m/s, 4 m/s, 5 m/s, and 6 m/s, respectively. Therefore, the secondary flow entering through the flexible tubes accounts for only a few percent of the total flow rate.

As discussed in previous studies (for instance Gad-el-Hak and Corrsin, 1974), injection in counter-flow direction leads to a higher static pressure drop, but the turbulence level is increased downstream of the grid, which was the central objective of the present project. First studies using only the counter-flow jets exiting directly from the fixed grid led to relatively low turbulence levels. In order to further increase the turbulence intensity, flexible tubes were later attached onto the orifices at the grid intersections, as shown in Fig. 2. Many tests were performed to find the most appropriate flexible elements for the purpose of turbulence enhancement (Szaszák et al., 2012). Variations of different parameters (tube material and rigidity, diameter, wall thickness, length…), as well as the effect of adding an extra weight at the free end of the tubes (which shifted the center of gravity, for the purpose of modified inertial behavior) were tested. Finally, the highest turbulence level and quality were obtained with the following parameters: tubes made out of silicone (type ST-EC-60-001, measured Young's modulus $E = 2.2$ MPa, tube material density $\rho_t = 1170$ kg/m^3), a total length of the silicone tubes of $l_0 = 60$ mm (from which the active length was 55 mm, the remaining 5 mm corresponding to the attachment length), inner diameter of $d_i = 1.2$ mm, a wall thickness of $w = 0.5$ mm, no extra weight at the tube end.

It is interesting to check the performance of the tubes from the point of view of similarity theory (Buckingham's Pi-theorem). The relevant parameters impacting tube movement have been listed above and take into account the material properties, all dimensions of the moving tubes, as well as the air mass flow rate through the moving tubes. Combining these parameters, three non-dimensional numbers are derived. The first two are simply geometric ratios, $C_t = w/d_i$, which is the relative thickness of the tube, and $C_a = l^*/d_i$, which describes the tube aspect ratio, where l^* is the distance of the common center of gravity of both tube and extra weight (if added), measured from the end of the orifice to which the active element is attached. In the final retained case (without extra weight), $l^* = 55/2 = 27.5$ mm. The third parameter involves not only material properties and dimensions of the tube, but also the air mass flow rate through the flexible tube. It is termed the tube mobility number C_m and is given by Eq. (1):

$$C_m = \rho_t E d_i^4 / \dot{m}^2, \tag{1}$$

where

> ρ_t: density of the material of the tube;
>
> E: Young's modulus of the tube;
>
> d_i: inner diameter of the tube;
>
> $\dot{m}$: air mass flow rate through each active element.

All material combinations tested in this project and leading to a noticeable tube movement (Szaszák et al., 2012) correspond to a relatively small range for these three parameters:

- $0.18 \leq C_t \leq 0.53$,
- $10 \leq C_a \leq 29.2$,
- $18\ 196 \leq C_m \leq 146\ 759$.

The best result (corresponding to the parameters listed above) was obtained for $C_t = 0.42$, $C_a = 22.9$, and $C_m = 28\ 600$. This is the configuration used for all the results shown in what follows.

It was then verified that the tubes behaved in a chaotic motion (see Video 1) by using a high-speed camera (Chronos 1.4 equipped with Fujian 35mm f/1.7 optics) at a frame rate of 2.359 kHz. During this experiment, the moving ends of two directly neighboring tubes were colored to facilitate image processing. The simultaneous movements of the two selected tubes were then extracted by means of a dedicated MATLAB script. Fig. 3 shows the corresponding trajectories of the two tube ends during a time period of 3.2 seconds. Due to the multiple interactions between the
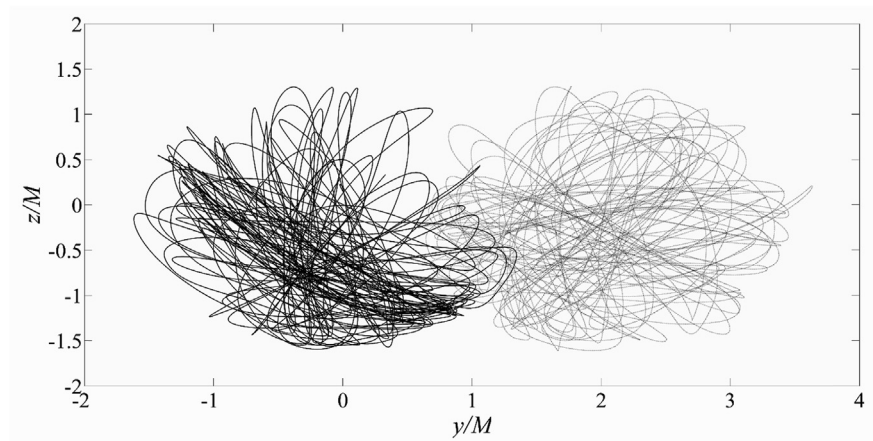

Fig. 3. Trajectories of two neighboring tube ends during a time period of 3.2 seconds, normalized by M. Left trajectory (continuous line) was plotted from the tube origin (0, 0), while the dashed line trajectory was plotted from (2M, 0), as in reality.

neighboring air jets, to the interaction with the incoming flow, and to the tube structure's own elastic motion, the resulting movements appear chaotic and uncorrelated. The calculated correlation coefficient between these two curves confirms our assumption. Using the standard function corr2 in MATLAB, a correlation coefficient of -0.0327 is obtained. This lies below the threshold value of 0.05 under which signals are considered as fully uncorrelated. Note that only the projected movements in the plane parallel to the camera image are shown here; perspective effects cannot be taken into account.

Using these trajectories it was further possible to assess the characteristic tip velocity of the moving tubes. With a single camera, only the in-plane velocity component (perpendicular to the streamwise direction) could be obtained. However, this is expected to be the dominating component for the tubes. Finally, peak tube velocities around 5 m/s were measured, a magnitude comparable to the mean streamwise velocity found further downstream in the test section. Gravity does not seem to impact strongly the direction of tube motion, due to the light weight of the tubes (only 172 mg for the active part) and to the high pressure applied.

4. Results

The central objective of this study was to compare the turbulence properties of the flow in passive and semi-active grid modes. The turbulence of the flow can be characterized by several quantities derived from the measured time-series of velocity components. In the following, different properties are discussed: kinetic energy of turbulence (k), turbulence intensity (T_u) in the streamwise direction, isotropy ratio (i), dissipation rate of turbulent kinetic energy (ε), Kolmogorov length scale (η), Taylor Reynolds number (Re_λ), and one-dimensional turbulence energy spectra ($E_u(\kappa)$). The evolution of these quantities along the centerline of the wind tunnel have been examined as a function of the distance from the grid. Additionally, the isotropy and homogeneity of the turbulent flow along horizontal and vertical lines in the core region of the test section were examined as well (see again Fig. 1).

4.1. Isotropy and uniformity

In order to compare passive and semi-active modes, measurements were first performed along horizontal and vertical lines in a plane parallel to the grid and placed $20M$ or $50M$ downstream (M2, shown as two red crosses in Fig. 1). For these measurements, a mean velocity of $U_{ref} = 4$ m/s was selected. Table 1 shows the mean values of the isotropy ratio $i = u_{rms}/v_{rms}$ for all measurement points. Very good values close to 1.0 are obtained when operating in semi-active mode. Close to the grid ($20M$), a higher value was found for i in passive mode. It is important to recall

Table 1. Averaged values of isotropy ratio.

	i_{20M} [-]	i_{50M} [-]
Passive mode	1.14	0.99
Semi-active mode	1.03	0.97

that the grid was installed downstream of the contraction, which may be a reason for this observation.

Similar values have been observed in other grid turbulence experiments, either active or passive. For instance, Kang et al. (2003) measured a value of 1.14 at a distance of $40M$ from the active grid. Gad-el-Hak and Corrsin (1974) reported a value of 1.11 at a distance of $46M$ in their jet-grid experiments. Makita (1991) reported $i = 1.19$ in the case of passive and $i = 1.22$ for an active grid at a distance of $50M$ from the grid.

For the present study, the value obtained when activating the secondary flow is of higher importance. It was found that, in the semi-active case, the mean isotropy value decreased to a low value of 1.03 at a distance of $20M$, which is very satisfactory. The isotropy profiles both in the horizontal and vertical directions for $U_{ref} = 4$ m/s, $x/M = 20$, semi-active grid, are depicted in Fig. 4b. Similar profiles can be found in Larssen and Devenport (2011) when applying a Makita-type active grid with rotating vanes.

Besides measurements parallel to the grid, the evolution of the isotropy values have been investigated as well along the centerline of the test section, downstream of the grid in the interval $10M$-$50M$ in both passive and semi-active modes (measurement setup M1, see Fig. 1). Corresponding values for $U_{ref} = 3$ m/s up to 6 m/s as a function of dimensionless downstream distance from the grid can be found in Fig. 4a.
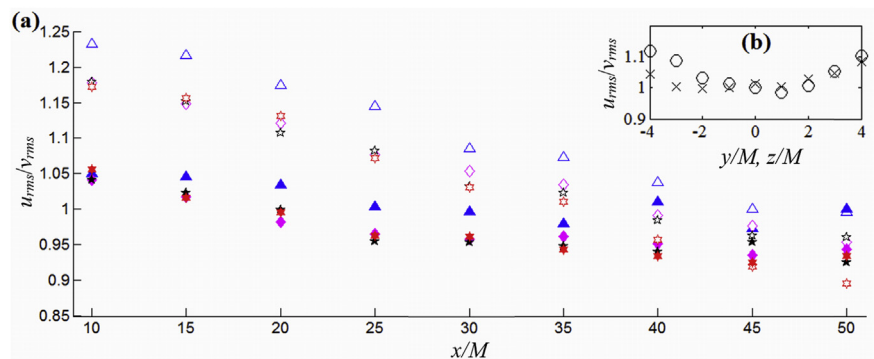

Fig. 4. (a) Isotropy ratio versus distance downstream of the grid. Passive mode: open markers; semi-active mode: filled markers (triangles: $U_{ref} = 3$ m/s; diamonds: $U_{ref} = 4$ m/s; pentagrams: $U_{ref} = 5$ m/s; hexagrams: $U_{ref} = 6$ m/s). (b) Profiles of isotropy ratio i in semi-active mode at $x/M = 20$ for $U_{ref} = 4$ m/s (crosses: horizontal measurement line; circles: vertical measurement line).

The values of the isotropy ratio noticeably decrease with increasing distance from the grid. A similar trend was reported by Kang et al. (2003) using a Makita-like grid design. Activating the semi-active mode, a lower isotropy value was obtained in most cases. Much better isotropy values were observed in semi-active mode close to the grid. Around $x/M = 50$, both passive and semi-active modes delivered a similar quality in terms of isotropy.

Many wind-tunnel studies require a very good approximation of homogeneous isotropic turbulence behind the grid. Hence, the degree of homogeneity of the velocity field achieved downstream of the grid is also an important requirement. The inhomogeneity can be quantified using the ratio of the time-averaged mean velocity values (U_m) along a line parallel to the grid to the reference streamwise mean velocity (U_{ref}). In previous jet-grid experiments, this value varied within a broad interval, from a minimum value of about 5% in the experiment by Gad-el-Hak and Corrsin (1974), where an individual throttle was applied on each jet to improve the homogeneity, about 10% in Liu et al. (1971), 15% in Mathieu and Alcaraz (1965) and in Teunissen (1969), up to the highest documented value of 30% in the experiment by Luxenberg and Wiskind (1969).

For the present experiments, the uniformity of the velocity was investigated using again the measurement setup M2 (Fig. 1), i.e., lines of size -4*M* to 4*M*, placed parallel to the grid at a downstream distance of either $x = 20M$ or $50M$. For $U_{ref} = 4$ m/s, Fig. 5 shows the uniformity of the velocity profile in both passive and semi-active modes, measured in the vertical (z) direction.

Fig. 5 shows that the activation of the jet grid leads to slightly higher inhomogeneity values. While in passive mode, at $x = 20M$, the inhomogeneity stays below 1.9%, this value increases to 3.4% in semi-active mode. At a distance of $x = 50M$, activation of the jet grid increases inhomogeneity up to 1.8%, compared to a value of 1.2% in passive mode. Nevertheless, all these values are lower than in many previous studies, as discussed above, and are sufficiently low to allow for accurate studies.
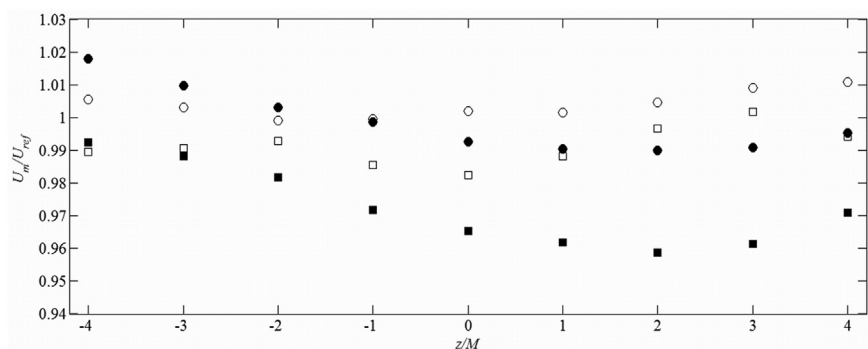

Fig. 5. Homogeneity profile measured in the vertical direction at $U_{ref} = 4$ m/s. Passive mode: open markers; semi-active mode: filled markers. Squares: $x/M = 20$; Circles: $x/M = 50$.

4.2. Turbulence intensity

The ratio between the root-mean-square (rms) value of the longitudinal fluctuating velocity component (u_{rms}) and the mean velocity (U_m) is known as the (longitudinal) turbulence intensity: $T_u = u_{rms}/U_m$. Fig. 6a shows the decay of this turbulence intensity downstream of the grid along the centerline of the test section. To avoid severe errors in the hot wire measurements caused by possibly negative streamwise velocity components in the near field of the grid (Krogstad, 2012), the centerline measurements were started from a distance of $10M$. The passive cases (open markers) for all conditions delivered nearly the same values at a given distance from the grid, in a range of 2.5%−7.7%, which means that in case of passive mode the bulk velocity U_{ref} is the scaling parameter for the turbulence intensity. This result is consistent with other passive grid experiments; in the case of square-mesh arrays of square bars, an empirical relation $T_u = 1.13(x/d)^{-5/7}$ exists between the streamwise turbulence intensity (T_u) and the downstream distance x/d, where d is the diameter of the square bar (Roach, 1987). From Fig. 6a, only minor differences appear between the measurements and the empirical curve; the reason for the slightly higher intensity may be the attached tubes.

In contrast with the passive mode, the results obtained with the semi-active grid show considerable differences; the values at a given distance from the grid do not fall on top of each other. This implies that for the semi-active mode, U_{ref} is not the only scaling parameter for turbulence production. Both the injected jets in counter-flow direction and the motion of the tubes increase the equivalent blockage induced by the grid, impacting turbulence production as well. In semi-active operation, the obtained intensity values noticeably decrease when increasing the mean inflow velocity, due to the corresponding normalization. While for $U_{ref} = 6$ m/s, values of T_u in the range of 4.5%−9.2% were found, these values
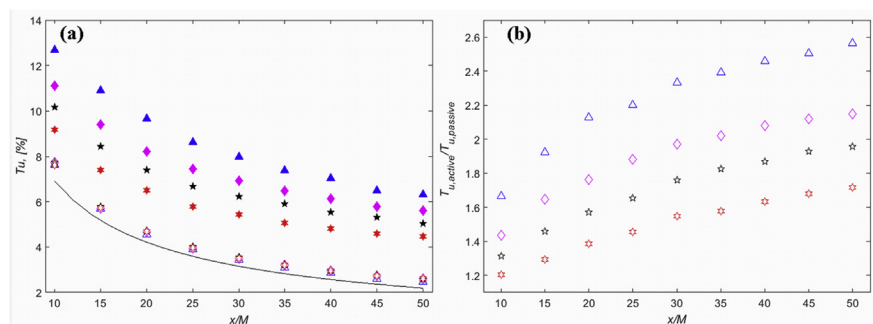

Fig. 6. (a) Decay of turbulence intensity along the centerline of the test section. Passive mode: open markers; semi-active mode: filled markers; line: empirical curve $T_u = 1.13(x/d)^{-5/7}$ from Roach (1987). (b) Ratio of turbulence intensity between semi-active and passive modes. In both cases, the mean inflow velocity was varied as follows: triangles: $U_{ref} = 3$ m/s; diamonds: $U_{ref} = 4$ m/s; pentagrams: $U_{ref} = 5$ m/s; hexagrams: $U_{ref} = 6$ m/s.

increase to 6.3%−12.7% for a lower inflow velocity of $U_{ref} = 3$ m/s. This demonstrates that the active grid was in particular able to generate high(er) turbulence fluctuations in a low-speed flow, which was one central objective of this project.

The effect of the active jets on turbulence intensity can be quantified by building the ratio of the corresponding semi-active and passive values, as shown in Fig. 6b. An increase in turbulence intensity by a large factor (between 1.2 and 2.6) is observed, in which the largest increase of turbulence intensity values corresponds to the slowest flow velocity ($U_{ref} = 3$ m/s) and the largest distance from the grid. As an order of magnitude, this figure shows that the turbulence intensity is roughly doubled in semi-active mode.

In order to check again the homogeneity of the obtained turbulence fields, the variations of the values of T_u at a fixed distance from the grid ($x = 20M$ or $50M$) were investigated along horizontal and vertical lines for $U_{ref} = 4$ m/s (configuration M2). For the passive grid, the measured variation for T_u was 4.4% and 2.9% at a distance of $20M$ and $50M$, respectively. In the semi-active grid mode, slightly higher values were obtained, namely 6.9% ($20M$) and 8.0% ($50M$), confirming the findings of the previous section.

4.3. Turbulence kinetic energy

The most important scalar quantity characterizing turbulence is probably the turbulent kinetic energy (k), i.e., the mean kinetic energy of the fluid per unit mass. Physically, the turbulent kinetic energy is computed from the velocity fluctuations. In our experiments, a 2-dimensional CTA probe was used, which allowed us to measure both the streamwise and one transversal (horizontal) velocity component simultaneously; the vertical velocity component was not investigated. As very often done in the literature concerning grid turbulence, it was assumed in this study that the transverse rms velocity fluctuations are almost identical ($v_{rms} \approx w_{rms}$). Starting from the general definition of k (e.g., Pope (2000)) the computation can then be simplified:

$$k \approx \frac{1}{2} \cdot \left(u_{rms}^2 + 2 \cdot v_{rms}^2 \right). \tag{2}$$

The approximation underlying Eq. (2) can be deemed acceptable here, recalling the low values of the isotropy factor i discussed in Section 4.1, particularly for the semi-active grid case (the most interesting one for the present study).

The measured values obtained with Eq. (2) along the centerline downstream of the grid for both passive and semi-active modes are plotted in Fig. 7a. In contrast to the previously discussed turbulence intensity, the mean inflow velocity has a significant influence on k, even in the passive mode. A higher mean velocity in the test section
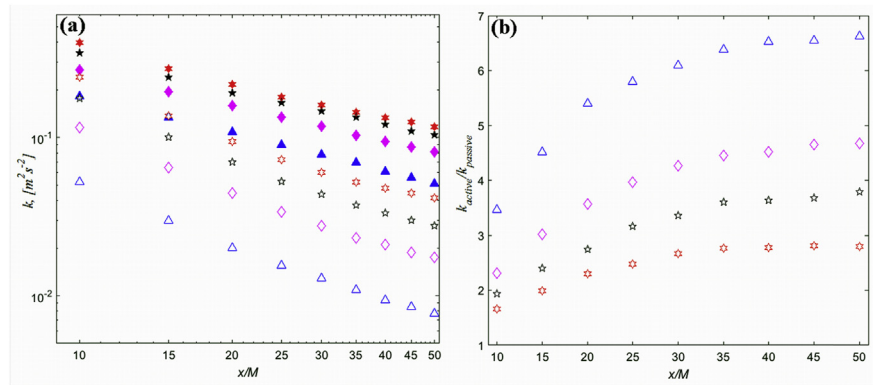
Fig. 7. (a) Evolution of the kinetic energy of turbulence along the centerline (log-log scale). Passive mode: open markers; semi-active mode: filled markers. (b) Ratio of turbulent kinetic energy between semi-active and passive mode. In both cases, the mean inflow velocity was varied as follows: triangles: $U_{ref} = 3$ m/s; diamonds: $U_{ref} = 4$ m/s; pentagrams: $U_{ref} = 5$ m/s; hexagrams: $U_{ref} = 6$ m/s.

(U_{ref}) always corresponds to higher values of k, as already observed, e.g., in the experiments by Kurian and Fransson (2009) and Danesh-Yazdi et al. (2015). Based on Fig. 7a, the semi-active grid (filled markers) always leads to flows with a much higher turbulent kinetic energy for the same primary flow velocity. The increase of k can be quantified by Fig. 7b, where the ratio of k_{active} to $k_{passive}$ is plotted. Confirming previous observations, the largest increase of turbulent kinetic energy (by a factor 6.6) was obtained for the slowest primary flow and at the largest distance from the grid ($50M$). This again demonstrates that 1) the active mode is particularly suitable to generate high turbulence levels in a slow incoming flow, and 2) the obtained turbulence levels decay at a slower pace compared to the passive case. When activating the grid, the increase of k is systematically higher at an increasing distance from the grid in the range investigated during this study.

4.4. Dissipation rate

Since there is no noticeable turbulent eddy production in the flow downstream of the grid (ignoring the direct neighborhood of the grid by remembering that all measurements start at $10M$), turbulence decays with increasing downstream distance due to viscous energy dissipation. The dissipation rate ε is another essential scalar used to characterize the generated turbulence. Observing again Fig. 7a, it is worth noting that the slopes corresponding to the semi-active operation mode of the grid have a different slope from those in the passive case. This indicates that the activation of the grid has an effect on the turbulent kinetic energy dissipation rate, as well. Assuming local isotropy in connection with Taylor's hypothesis, as done in many other studies considering grid turbulence (e.g., Larssen and Devenport (2002)), the dissipation rate can be computed from Eq. (3) (Pope, 2000):

$$\varepsilon = \int_0^\infty 2\nu\kappa^2 E(\kappa)d\kappa, \tag{3}$$

where ν is the kinematic viscosity of air, κ is the wave number, and $E(\kappa)$ is the spectrum of the total energy that was computed from the measured spectrum $E_u(\kappa)$ of the u component and $E_v(\kappa)$ of the v component using Eq. (4), while applying again the assumption that transverse rms velocity fluctuations are almost identical ($v_{rms} \approx w_{rms}$). Here, $\kappa = 2\pi f/U_{ref}$, where f is the frequency (Hz).

$$E(\kappa) = \frac{1}{2}[E_u(\kappa) + 2E_v(\kappa)] \tag{4}$$

To cross-check the calculated energy spectrum $E(\kappa)$, the turbulence kinetic energy values (k) calculated previously from velocity fluctuations were compared with that derived from Eq. (5) (Pope, 2000):

$$k = \int_0^\infty E(\kappa)d\kappa . \tag{5}$$

The resulting deviations have been found to be systematically lower than 4%.

The dissipation rate ε for both passive and semi-active modes of the grid along the centerline as a function of downstream distance from the grid (measurement line M1) is depicted in Fig. 8.

As observed from Fig. 8, the rate of energy dissipation is greater near the grid in both passive and semi-active cases, confirming observations from the literature, e.g., by Kang et al. (2003). Furthermore, the mean inflow velocity has a higher effect on this quantity closer to the grid, while the values of the dissipation rate appear to collapse onto one another further downstream, especially in passive mode. In the entire investigated range, the activation of the grid results in higher values for the
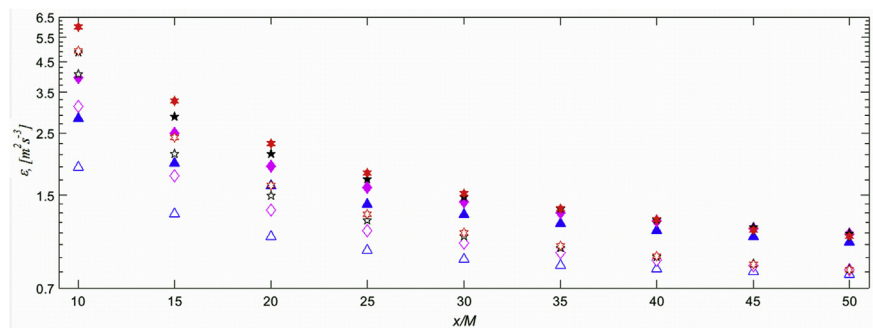

Fig. 8. Evolution of the turbulent kinetic energy dissipation rate ε along the centerline of the test section (log-log scale). Passive mode: open markers; semi-active mode: filled markers. The mean inflow velocity was varied as follows: triangles: $U_{ref} = 3$ m/s; diamonds: $U_{ref} = 4$ m/s; pentagrams: $U_{ref} = 5$ m/s; hexagrams: $U_{ref} = 6$ m/s.

dissipation rate. In order to compare our results with other experimental data, the dimensionless dissipation constant $C_\varepsilon = \varepsilon L u_{rms}^{-3}$ was calculated, where L is the integral length scale derived from the autocorrelation function of the longitudinal velocity component u. Both for passive and semi-active cases, values of C_ε follow fairly well the power law with a positive exponent as a function of downstream distance from the grid, as shown in Fig. 9.

According to Fig. 9 the values corresponding to passive operation are systematically higher than the corresponding values found in semi-active mode. These results agree with the findings of the jet grid experiment by Gad-el-Hak and Corrsin (1974). In their experiment, with zero injection (passive mode), values of $C_\varepsilon = 2.43-2.63$ (for $x/M = 30-46$) were measured, higher than for counterflow injection, for which $C_\varepsilon = 1.30-1.44$ was found. In the present experiment, values of C_ε between 0.31 and 2.99 have overall been obtained in semi-active mode, depending on axial position and mean inflow velocity.

Another important observation is the phenomenon of increasing dissipation coefficient C_ε with decreasing Taylor Reynolds number Re_λ (see also Section 4.6). Based on the literature dealing with this issue, e.g. Burattini et al. (2006) or Goto and Vassilicos (2016), this phenomenon may arise either in low Reynolds number flow, where viscous effects are directly effective, or from non-equilibrium turbulence. In both cases a linear relation $C_\varepsilon \sim Re_\lambda^{-1}$ has been observed in previous studies. Our results corroborate these findings. Computing the linear regression for all measurement series, the correlation coefficients r^2 (a measure for the reliability of a linear regression) lie within $0.87-0.96$ for all passive cases, and in the range of $0.97-0.99$ for the active grid. These high values, very close to 1, confirm the validity of the linear relationship $C_\varepsilon \sim Re_\lambda^{-1}$ in the present investigation.
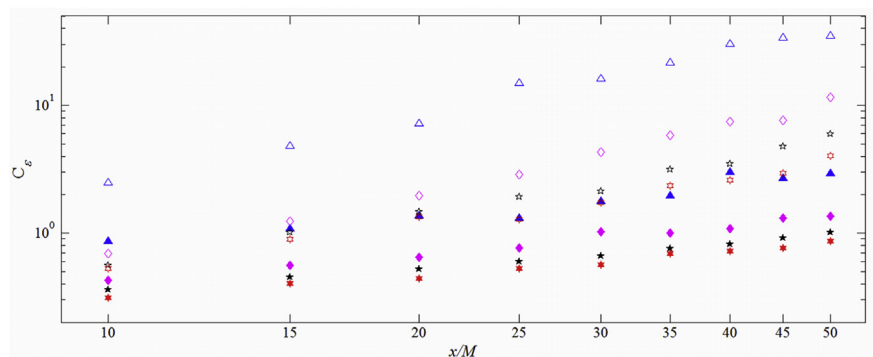

Fig. 9. Evolution of the dissipation constant C_ε along the centerline of the test section (log-log scale). Passive mode: open markers; semi-active mode: filled markers. The mean inflow velocity was varied as follows: triangles: $U_{ref} = 3$ m/s; diamonds: $U_{ref} = 4$ m/s; pentagrams: $U_{ref} = 5$ m/s; hexagrams: $U_{ref} = 6$ m/s.

4.5. Kolmogorov microscale

The Kolmogorov scale characterizes the smallest dissipative eddies in turbulent flow. It cannot be measured directly by CTA. Based on Kolmogorov theory, the statistics associated with small-scale properties are universally and uniquely determined by the kinematic viscosity of the fluid (ν) and the previously introduced rate of energy dissipation per unit mass (ε). Thus, it is possible to introduce a unique length, the so-called Kolmogorov length scale η in Eq. (6), which characterizes dissipation in turbulent flow:

$$\eta = \left(\frac{\nu^3}{\varepsilon}\right)^{1/4}. \tag{6}$$

In the present case, the viscosity of the fluid is constant, as is the temperature. Hence, the evolution of the Kolmogorov microscale is directly correlated to the modifications of the dissipation rate shown in Fig. 8. Fig. 10 shows the evolution of η estimated from Eq. (6). For both the passive and the semi-active grid, a higher mean inflow velocity always leads to a lower value of the Kolmogorov scale, confirming the results from the literature, e.g., Gad-el-Hak and Corrsin (1974), Kurian and Fransson (2009), or Larssen and Devenport (2002). Using the semi-active mode, the obtained Kolmogorov scale is reduced, as in the work by Makita (1991). The jet-grid experiments by Gad-el-Hak and Corrsin (1974) delivered almost the same values at $x/M = 30$: in passive mode, a value of 0.31 mm was calculated (compared to the present value of 0.29 mm for $U_{ref} = 6$ m/s in passive mode), while in counterflow injection ("semi-active" grid), $\eta = 0.29$ mm was documented, compared with the presently measured value of 0.27 mm.

4.6. Taylor Reynolds number

Another important quantity that characterizes grid turbulence is the Taylor Reynolds number Re_λ, which is related to the Taylor microscale λ_g and the characteristic
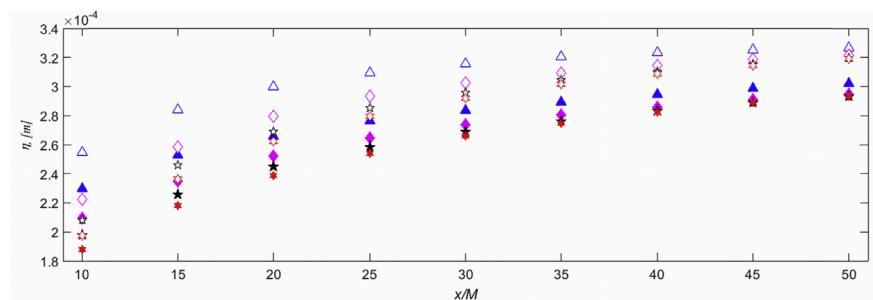

Fig. 10. Kolmogorov microscale as a function of normalized downstream distance from the grid. Passive mode: open markers; semi-active mode: filled markers. The mean inflow velocity was varied as follows: triangles: $U_{ref} = 3$ m/s; diamonds: $U_{ref} = 4$ m/s; pentagrams: $U_{ref} = 5$ m/s; hexagrams: $U_{ref} = 6$ m/s.

velocity $k^{1/2}$. Following again for instance Pope (2000), there is a well-defined relationship between the Taylor Reynolds number and the turbulence kinetic energy k, dissipation rate ε and viscosity ν as shown by Eq. (7):

$$\text{Re}_\lambda = \left(\frac{20}{3} \cdot \frac{k^2}{\varepsilon\nu} \right)^{1/2}. \tag{7}$$

Due to limitations in wind tunnel size and mean flow velocity in most laboratories, Taylor Reynolds numbers of at most a few hundred can usually be reached by using passive grids. Mohamed and LaRue (1990) reached values of Re_λ in the range of $28.37-41.60$ at a downstream distance of $40M$ from their biplane passive grid constructed of polished aluminum rods ($M = 25.4$ mm, $D_{rod} = 4.76$ mm). Comte-Bellot and Corrsin (1966) acquired Re_λ values in the range of $36-72$. Far greater values were obtained in the experiments by Kistler and Vrebalovich (1966): using a wind tunnel with a cross section of 2.59 m × 3.51 m equipped with a passive grid, at a free stream velocity of 61 m/s and controlling the pressure as well, peak Re_λ values of approximately 670 were reached. One central objective of the present project was to obtain a larger Taylor Reynolds numbers even for limited inflow velocities and in wind tunnels with a limited size. The obtained values of Re_λ along the centerline of the test section for different reference velocities in both passive and semi-active modes are presented in Fig. 11a, while the ratio between Re_λ in semi-active and passive mode is displayed in Fig. 11b.

Several conclusions can be drawn from Fig. 11a. The values of Re_λ decreased as expected with the downstream distance and increased with mean inflow velocity. In passive mode, low Re_λ values were found due to the low inflow velocities and to the small size of the wind tunnel cross section (0.5 m × 0.5 m). Results of the jet grid experiment performed by Gad-el-Hak and Corrsin (1974) show a good qualitative agreement; for a mean velocity of 9.02 m/s, Taylor Reynolds numbers of 105
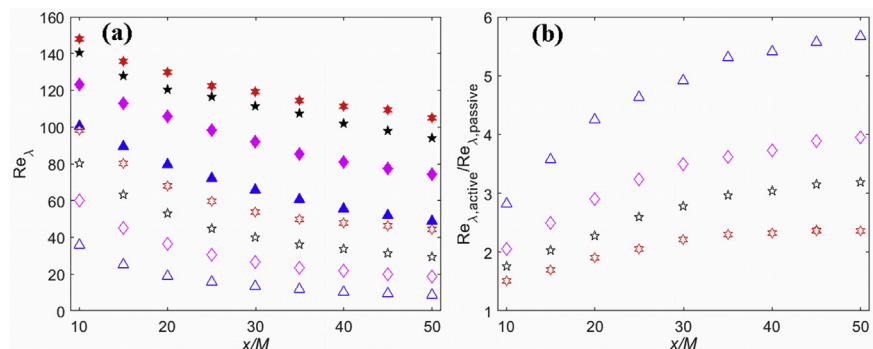

Fig. 11. (a) Taylor Reynolds number as a function of normalized distance from the grid. Passive mode: open markers; semi-active mode: filled markers. (b) Ratio of Taylor Reynolds number between semi-active and passive mode. In both cases, the mean inflow velocity was varied as follows: triangles: $U_{ref} = 3$ m/s; diamonds: $U_{ref} = 4$ m/s; pentagrams: $U_{ref} = 5$ m/s; hexagrams: $U_{ref} = 6$ m/s.

(passive) and 150 (jet mode with counterflow injection) were obtained at $x/M = 30$, leading to a ratio of 1.43. At the same distance, setting only $U_{ref} = 6$ m/s (the maximum velocity accessed in the present study), values of 54 (passive mode) and 119 (semi-active mode) were measured, corresponding to an even higher increase by a factor of about 2.2. As discussed previously, the relative increase is higher at a lower mean inflow velocity and at a larger downstream distance from the grid (Fig. 11b). For $U_{ref} = 3$ m/s at $x/M = 50$, a maximum increase in Taylor Reynolds number by a factor of 5.66 was measured.

4.7. Energy spectra

Fig. 12a shows the energy spectra of the u component measured at $x/M = 30$ downstream of the grid for both passive and semi-active modes and for the four different reference velocities. Spectra are first shown in dimensional form as E_u versus κ, where E_u is the longitudinal one-dimensional power spectrum and κ is the longitudinal wavenumber, with units of m^{3}s^{-2}, respectively m^{-1}. The wavenumber corresponding to the tunnel width is 12.57 m^{-1}. Keeping the reference inflow velocity U_{ref} constant (compare lines with same symbols), the semi-active mode (filled markers) systematically lead to a much higher turbulent kinetic energy k (i.e., a greater area under the E_u curve) compared to the passive case, confirming the results in Fig. 7. Even more important, activation of the grid results in a noticeably wider inertial range following the expected -5/3 power-law (straight solid lines in Fig. 12), as also shown by the compensated spectra plotted as inset in Fig. 12(b).
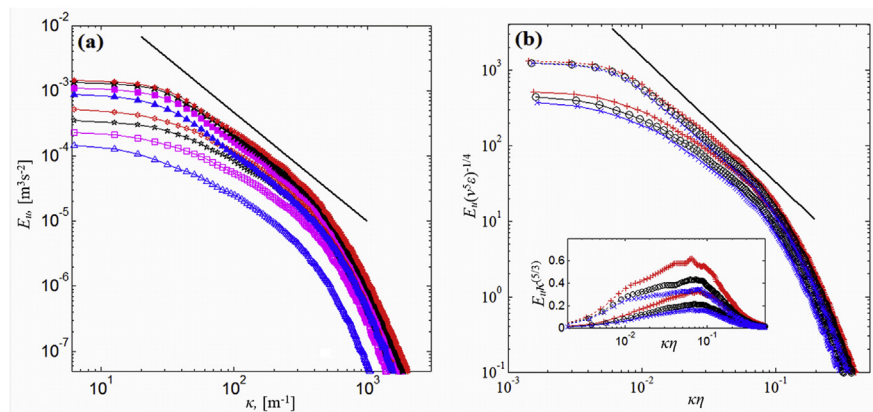

Fig. 12. (a) Longitudinal one-dimensional energy spectra at $x/M = 30$. Passive mode: open markers; semi-active mode: filled markers. In both cases, the mean inflow velocity was varied as follows: triangles: $U_{ref} = 3$ m/s; diamonds: $U_{ref} = 4$ m/s; pentagrams: $U_{ref} = 5$ m/s; hexagrams: $U_{ref} = 6$ m/s. (b) Normalized longitudinal energy spectra for $U_{ref} = 6$ m/s at $x/M = 30$ (plus signs), 40 (circles), and 50 (crosses). Passive mode: continuous lines; semi-active mode: dashed lines. The straight solid lines correspond to the -5/3 power law. The inset shows the compensated spectra.

In Fig. 12b, the effect of the downstream distance is illustrated in both passive and semi-active modes. Here, the wave number κ and the spectrum E_u were each normalized by the Kolmogorov length scale η, by the kinematic viscosity ν, and the dissipation rate ε. Again, the positive impact of activation is clearly visible: using the semi-active mode, the inertial range of the spectra becomes broader and turbulence decay with downstream distance is much less pronounced.

5. Conclusion

A novel, robust, and cost-effective semi-active turbulence grid was described and experimentally investigated in this paper. Using hot-wire anemometry, the flow downstream of the grid has been characterized in a systematic manner, both in passive and in semi-active mode, while varying the inflow velocity. Results presented in this paper are consistent with those found in the scientific literature. Activation of the grid had very significant effects on all turbulence parameters: a considerable increase was achieved for turbulence intensity, turbulent kinetic energy, and Reynolds numbers. Additionally, the semi-active grid delivered spectra corresponding much closer to fully-developed turbulence, with a broader inertial range. Excellent isotropy and homogeneity of the generated turbulence were observed. During all the tests, the proposed grid behaved in a robust manner, with no observed damage. For all of these reasons, the authors believe that the semi-active grid first described in this work might provide a suitable alternative of turbulence generation for many other groups working with wind tunnels. In principle, it could also be used for any other open air flows, as well as in liquid flows, for instance in a water channel.

Declarations

Author contribution statement

N. Szaszák, C. Roloff, R. Bordás: Conceived and designed the experiments; Performed the experiments; Analyzed and interpreted the data; Wrote the paper.

P. Bencs: Conceived and designed the experiments; Performed the experiments; Wrote the paper.

S. Szabó: Conceived and designed the experiments.

D. Thévenin: Conceived and designed the experiments; Wrote the paper.

Funding statement

GINOP-2.3.4-15-2016-00004 project, aimed to promote the cooperation between the higher education and the industry.

Competing interest statement

The authors declare no conflict of interest.

Additional information

Supplementary content related to this article has been published online at https://doi.org/10.1016/j.heliyon.2018.e01026.

References

Antonia, R.A., Lavoie, P., Djenidi, L., Benaissa, A., 2010. Effect of a small axisymmetric contraction on grid turbulence. Exp. Fluid 49 (1), 3−10.

Aufderheide, T., Bode, C., Friedrichs, J., Kozulovic, D., 2014. The generation of higher levels of turbulence in a low-speed cascade wind tunnel by pressurized tubes. In: 11th World Congress on Computational Mechanics (WCCM XI).

Bordás, R., Hagemeier, T., Wunderlich, B., Thévenin, D., 2011. Droplet collisions and interaction with the turbulent flow within a two-phase wind tunnel. Phys. Fluids 23 (085105), 1−11.

Bordás, R., Roloff, C., Thévenin, D., Shaw, R., 2013. Experimental determination of droplet collision rates in turbulence. New J. Phys. 15 (045010), 1−31.

Burattini, P., Lavoie, P., Agrawal, A., Djenidi, L., Antonia, R.A., 2006. Power law of decaying homogeneous isotropic turbulence at low Reynolds number. Phys. Rev. 73 (066304), 1−7.

Charnay, G., 1969. Etude D'une Couche Limite Perturbée Par Une Turbulence Extérieure. Ecole Centrale de Lyon, Lab. de Mécanique des Fluides. Ph.D. Thesis.

Comte-Bellot, G., 1971. Simple eulerian time correlation of full- and narrow-band velocity signals in grid-generated, isotropic turbulence. J. Fluid Mech. 48 (2), 273−337.

Comte-Bellot, G., Corrsin, S., 1966. The use of a contraction to improve the isotropy of grid-generated turbulence. J. Fluid Mech. 25 (4), 657−682.

Danesh-Yazdi, A.H., Goushcha, O., Elvin, N., Andreopoulos, Y., 2015. Fluidic energy harvesting beams in grid turbulence. Exp. Fluid 56 (161).

Fransson, J.H.M., Matsubara, M., Alfredsson, P.H., 2005. Transition induced by free-stream turbulence. J. Fluid Mech. 527, 1−25.

Gad-el-Hak, M., Corrsin, S., 1974. Measurements of the nearly isotropic turbulence behind a uniform jet grid. J. Fluid Mech. 62 (1), 115−143.

Goepfert, C., Marié, J.L., Chareyron, D., Lance, M., 2010. Characterization of a system generating a homogeneous isotropic turbulence field by free synthetic jets. Exp. Fluid 48 (5), 809−822.

Goto, S., Vassilicos, J.C., 2016. Unsteady turbulence cascades. Phys. Rev. 94 (053108), 1−11.

Guillon, O., 1968. Essais de mise au point d'une grille active à grandes mailles. Ecole Centrale de Lyon, Lab. de Mécanique des Fluides, Ph.D. Thesis.

Hearst, R. Jason, Lavoie, Philippe, 2015. The effect of active grid initial conditions on high Reynolds number turbulence. Exp. Fluid 56 (10), 185.

Hwang, W., Eaton, J.K., 2004. Creating homogeneous and isotropic turbulence without a mean flow. Exp. Fluid 36 (3), 444−454.

Kang, H.S., Chester, S., Meneveau, C., 2003. Decaying turbulence in an active-grid-generated flow and comparisons with large-eddy simulation. J. Fluid Mech. 480, 129−160.

Kistler, A.L., Vrebalovich, T., 1966. Grid turbulence at large Reynolds numbers. J. Fluid Mech. 26 (1), 37−47.

Krogstad, P.A., 2012. Turbulent decay in the near field of multi-scale and conventional grids. Int. J. Heat Fluid Flow 35, 102−108.

Kurian, T., Fransson, J.H.M., 2009. Grid-generated turbulence revisited. Fluid Dynam. Res. 41, 021403.

Larssen, J.V., Devenport, W.J., 2002. The Generation of High Reynolds Number Homogeneous Turbulence. In: 32nd AIAA Fluid Dynamics Conference and Exhibit, St. Louis.

Larssen, J.V., Devenport, W.J., 2011. On the generation of large-scale homogeneous turbulence. Exp. Fluid 50, 1207−1223.

Ling, S.C., Wan, C.A., 1972. Decay of isotropic turbulence generated by a mechanically agitated grid. Phys. Fluids 15 (8), 1363.

Liu, J.C.H., Greber, I., Wiskind, H.K., 1971. Experimental Measurements of Grid Injection Turbulent Flows. Case Western Reserve University Tech. Rep. FTAS/TR-70-53.

Luxenberg, D.S., Wiskind, K., 1969. Some Effects of Air Injection on the Turbulence Generated by a Bi-planar Grid. Case Western Reserve University Tech. Rep. FTAS/TR-69-42.

Makita, H., Miyamoto, S., 1983. Generation of high intensity turbulence and control of its structure in a low speed wind tunnel. In: Proc. 2nd Asian Congress on Fluid Mechanics Beijing, China, pp. 101–106.

Makita, H., 1991. Realization of a large-scale turbulence field in a small wind tunnel. Fluid Dynam. Res. 8, 53–64.

Mathieu, J., Alcaraz, E., 1965. "Réalisation d'une soufflerie à haut niveau de turbulence," CR. Acad. Sci. 261, 2435.

Mohamed, M.S., LaRue, J.C., 1990. The decay power law in grid-generated turbulence. J. Fluid Mech. 219, 195–214.

Mydlarski, L., Warhaft, Z., 1996. On the onset of high-Reynolds-number grid-generated wind tunnel turbulence. J. Fluid Mech. 320, 331–368.

Mydlarski, L., 2017. A turbulent quarter century of active grids: from Makita (1991) to the present. Fluid Dynam. Res. 49 (6), 061401.

Ozono, S., Miyagi, H., Wada, K., 2007. Turbulence generated in active grid mode using a multi-fan wind tunnel. J. Fluid Sci. Technol. 2 (3), 643–654.

Pope, S.B., 2000. Turbulent Flows. Cambridge Univ. Press.

Roach, P.E., 1987. The generation of nearly isotropic turbulence by means of grids. Int. J. Heat Fluid Flow 8 (2), 82–92.

Sakai, Y., Watanabe, T., Kamohara, S., Kushida, T., Nakamura, I., 2001. Simultaneous measurements of concentration and velocity in a CO2 jet issuing into a grid turbulence by two-sensor hot-wire probe. Int. J. Heat Fluid Flow 22 (3), 227–236.

Sato, H., Saito, H., 1974. In: Proc. 6th Turbulence Symposium, 103 [in Japanese].

Simmons, L.F.G., Salter, C., 1934. Experimental investigation and analysis of the velocity variations in turbulent flow. Proc. R. Soc. London, Ser. A 145 (854), 212–234.

Szaszák, N., Bordás, R., Mátrai, Z., Thévenin, D., Szabó, S., 2012. Experimental characterization of a cost-effective semi-active grid for turbulence stimulation. In: Proc. Conference on Modelling Fluid Flow (CMFF'12), Budapest, Hungary, pp. 362–368.

Szaszák, N., Bencs, P., Szabó, S., 2017. Determining turbulent properties in grid-generated turbulence based on hot-wire data. In: Proc. Int. Conf. on Innovat. Technol. (IN-Tech), Ljubljana, Slovenia, pp. 73–76.

Tassa, Y., Kamotani, Y., 1975. Experiments on turbulence behind a grid with jet injection in downstream and upstream direction. Phys. Fluids 18 (4), 411.

Teunissen, H.W., 1969. An ejector-driven wind tunnel for the generation of turbulent flows with arbitrary mean velocity profile. In: UTIAS Tech. Note 133. University of Toronto.

Townsend, A.A., 1954. The uniform distortion of homogeneous turbulence. Q. J. Mech. Appl. Math. 7 (1), 104−127.

Variano, E.A., Bodenschatz, E., Cowen, E.A., 2004. A random synthetic jet array driven turbulence tank. Exp. Fluid 37, 613−615.

Villermaux, E., Gagne, Y., Hopfinger, E.J., Sommeria, J., 1991. Oscillatory instability and genesis of turbulence behind a high solidity grid. Eur. J. Mech. B Fluid 10 (4), 427−439.

Vonlanthen, R., Monkewitz, P.A., 2011. A novel tethered-sphere add-on to enhance grid turbulence. Exp. Fluid 51, 579−585.

Weitemeyer, Stefan, et al., 2013. Multi-scale generation of turbulence with fractal grids and an active grid. Fluid Dynam. Res. 45 (6), 061407.